A MARTINI coarse-grained model of a thermoset polyester coating

ARTICLE *in* MACROMOLECULES · AUGUST 2011

Impact Factor: 5.8 · DOI: 10.1021/ma200788a

Macromolecules

ARTICLE

pubs.acs.org/Macromolecules

A MARTINI Coarse-Grained Model of a Thermoset Polyester Coating

Giulia Rossi,[*,†] Ioannis Giannakopoulos,[‡] Luca Monticelli,[§,◆,¶] Niko K. J. Rostedt,[⊥] Sakari R. Puisto,[⊥] Chris Lowe,[∥] Ambrose C. Taylor,[‡] Ilpo Vattulainen,[▽,#] and Tapio Ala-Nissila[†,○]

[†]Department of Applied Physics, Aalto University School of Science, P.O. Box 11000, FI-00076 AALTO, Helsinki, Finland

[‡]Department of Mechanical Engineering, Imperial College London, South Kensington Campus, London 6 SW7 2AZ, United Kingdom

[§]INSERM, UMR-S 665, DSIMB, 6 rue Alexandre Cabanel, 75015 Paris, France

[⊥]Matox Ltd., Pembroke House, 36-37 Pembroke Street, Oxford OX1 1BP, United Kingdom

[∥]Becker Industrial Coatings Ltd., Goodlass Road, Speke, Liverpool L24 9HJ, United Kingdom

[▽]Department of Physics, Tampere University of Technology, P.O. Box 692, FI-33101, Tampere, Finland

[#]MEMPHYS, Center of Biomembrane Physics, University of Southern Denmark, Campusvej 55, DK-5230 Odense M, Denmark

[○]Department of Physics, Brown University, P.O. Box 1843, Providence, Rhode Island 02912-1843, United States

[◆]Université Paris Diderot −Paris 7, UFR Sciences du Vivant, Paris, France

[¶]INTS, Paris, France

Supporting Information

ABSTRACT: We hereby present a coarse-grained model of a typical polyester resin for coil coating applications. We validate the model via comparison with experimental data. The interactions between coarse-grained particles are described by the MARTINI force-field [Marrink et al. et al. J. Phys. Chem. B 2007, 11, 7812]. Our model and molecular dynamics simulation protocols include the description of a hardener and the formation of cross-links between the hardener and the polyester resin. We perform experimental tests on the thermodynamic and mechanical properties of the system, and compare them with molecular dynamics simulations. The model estimates the glass transition temperature of the coating within 30 K of the experimental measurement. The model captures correctly the broadening effect of cross-linking on the glass transition, and on the temperature dependence of the elastic response of the polyester resin.

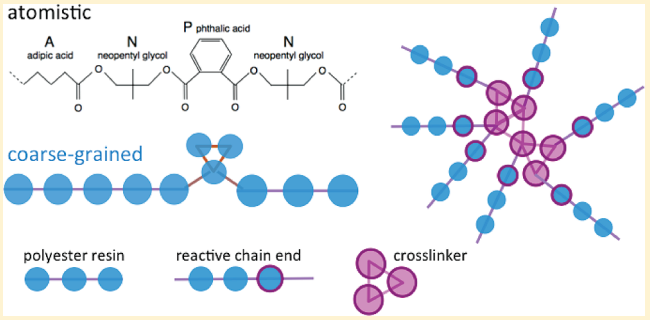

INTRODUCTION

Prepainted steel is used in a variety of applications, ranging from the construction industry to automotive manufacturing. Coil coatings are organic polymer coatings which need to satisfy strict requirements in terms of mechanical performance. They have to be formable, to withstand processing in harsh conditions without cracking, and they need to be hard, so as to resist scratching during and after their installation.

Among coil coatings, polyester coatings are quite common. Most coating polyesters have a relatively low molecular weight (M_W) and are amorphous.[1] Commonly they are made from mixtures of diols, triols, and dibasic acids. Coating applications require the low-M_W polymer chains to be thermoset, that is cross-linked by thermal activation of the chemical bonds between the polymer chains and a cross-linking agent. Thermoset systems allow for better adhesion to metal substrates and better impact resistance. The optimization of the coating properties for these industrial applications is generally achieved by controlling the fine details of both the resin and paint formulations, often through expensive and time-consuming trial-and-error procedures.

Computer modeling can be a useful complement to experimental investigation, speeding up the exploration of alternative formulations and providing novel insight on the system. In order to relate the fine physical (structural and dynamical) and chemical features of the polymer resin to the mechanical performance of the coating, we need a molecular description including sufficient chemical detail. Unfortunately, despite ever increasing computational resources, simulations of polymer melts from atomistic detail are subject to stringent limitations to the time and length scales of the phenomena that can be observed.[2−4] Simulating the mechanical response of a polymeric material requires simulations of tens of microseconds over length scales of tens of nanometers,[5,6] currently not accessible with fully atomistic descriptions.

Coarse-grained (CG) approaches help to overcome these limitations, yet retaining a molecular-level description of the polymer resin. Coarse-graining means grouping atoms from the all-atom

Received: April 5, 2011
Revised: June 23, 2011
Published: July 08, 2011

description of the molecules into superatoms, or beads, in such a way as to reduce the number of particles to be dealt with. Coarse-graining affects the nature of interparticle interactions, too, making them softer. Thus, larger timesteps can be used during molecular dynamics (MD) simulations, and intermolecular friction is normally decreased. All these elements allow for a description of the resin dynamics on larger time and length scales than by atomistic simulations.

Coarse-grained models of polymers have been used to investigate the mechanical response of polymer resins, often by means of molecular dynamics simulations. Since the 1990s, the popular bead−spring model by Kremer and Grest[7] and many variations of the same idea have been applied in the field. These models do not aim at describing any particular polymer system, but can faithfully reproduce the most general structural and dynamical features of (entangled) polymer melts. Gersappe and Robbins[8] focused on the mechanical failure of polymer adhesives, while Baljon and Robbins[9] studied crazing in polymer glasses. More recently, computational techniques such as MD have been getting closer and closer to experimentally relevant time and length scales. Good qualitative agreement has been found between the outcomes of creep tests in experiments and simulations.[10] MD simulations are currently being used to elucidate the mechanisms underlying experimental observations, such as the enhanced molecular mobility observed during the deformation of a polymer glass.[10−12]

Chemically specific CG models of polymers have been developed, as well (please see Rossi et al.[13] and references therein), with the aim to reproduce structural, dynamical and, to some extent, thermodynamic features of specific polymer systems. Nevertheless, the inclusion of several different chemical moieties into CG models is a challenge, and it often complicates considerably the model development and validation.

In this paper we present the development of a coarse-grained model of a typical polyester resin for coil coating applications. We validate the model by comparing the thermodynamic and mechanical properties obtained *in silico* to experimental data. For this purpose differential scanning calorimetry (DSC), dynamic mechanical analysis (DMA) and tensile tests at different temperatures were performed on samples of a formulation similar as that studied computationally.

We have adopted a MARTINI-based approach to coarse-graining. MARTINI is a coarse-grained model originally developed for lipids and detergents,[14,15] later extended to proteins,[16] lipoproteins,[17,18] sugars,[19] and fullerenes.[20] The viability of its coarse-graining approach for polymers has been recently tested on a few benchmark systems, for both bio-[21] and nonbio-applications.[22] The MARTINI model of polystyrene recently developed by Rossi et al.[13] has been shown to perform well in terms of reproduction of long-range structural properties of the melt, temperature transferability and compatibility with different solvent environments. In this paper we present the first application of MARTINI to the modeling of a polyester resin with the potential to directly impact on industrial-scale applications.

In the context of the CG modeling of polymer resins, an aspect that calls for special attention is the modeling of cross-links. Several alternative protocols for the MD simulation of cross-link formation in polymer networks have been proposed,[22−30] starting from the pioneering work of Duering et al.,[31,32] The cross-linking reaction in thermoset materials is a complex dynamic process which involves the polymer resin, one or more catalytic agents, the cross-linker molecules and the solvents, which evaporate

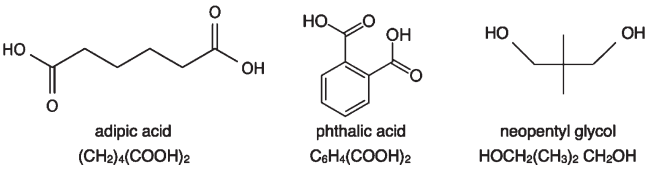

Figure 1. Chemical structures of the resin monomers.

while the reaction takes place at high temperature. Such a level of complexity, combined with the intrinsic limitations of classical potentials in describing the formation and breaking of chemical bonds, suggests to simplify the description of the reaction stage, and to focus on the characterization of the properties of the already formed cross-linked network. Here, we propose a simulation protocol that aims at mimicking at best the experimental thermosetting procedures for typical coil coating formulations. The protocol includes the possibility to treat partially and fully cross-linked systems, as well as the formation of bonds between cross-linker molecules (self-condensation).

In the section Model and Methods, we describe the chemical composition and connectivity of the chosen polyester system, the force-field parametrization and optimization, and our strategy to include cross-linking agents into the model. Experimental methods are described in the section Experimental Methods. In the Results section, we present the results of the structural, thermodynamical and mechanical characterization of our coating. The experimental data are presented in the section Experimental Characterization and computational results in the section MD Simulations. The overall model performance, and a comparison with the accompanying experimental data, are discussed in the Discussion section. In the Conclusions, we describe ongoing and future applications of the model, aimed at establishing direct connections between the molecular structure and dynamics of thermoset polymer nanocomposites and their mechanical performance.

MODEL AND METHODS

Coarse-Grained Model of the Polyester Resin. As a basic coil coating resin formulation, we chose to model a polyester composed of two dicarboxylic acids, adipic acid ($(CH_2)_4(COOH)_2$, IUPAC name hexanedioic acid) and phthalic acid ($C_6H_4(COOH)_2$, IUPAC name benzene-1,2-dicarboxylic acid), and a diol, neopentyl glycol ($HOCH_2\ (CH_3)_2CH_2OH$, IUPAC name 2,2-dimethylpropane-1,3-diol). We refer to them as to A, P, and N units, respectively. Their chemical structures are shown in Figure 1. Chains resulting from the esterification of the acids with neopentyl glycol monomers can be thus thought of as sequences of dimers, AN and PN. Two connected dimers, forming the ANPN sequence, are shown in Figure 2. We use this segment to illustrate how we map our CG model onto the atomistic description of the polyester resin.

Mapping. In the MARTINI approach, mapping of CG beads onto atoms is not uniquely defined, and usually a few alternatives are possible. The nonbonded interactions of MARTINI beads are parametrized based on their free energy of transfer between water and octanol (and other organic solvents, whenever possible). This criterion, adopted in the original MARTINI parametrization,[14,15] has led us to split ideally our polyester chain into chemical moieties characterized by different polarity, and then associate to each of them the most appropriate MARTINI bead type (for a detailed description of MARTINI types, please refer to the latest MARTINI release[15]).

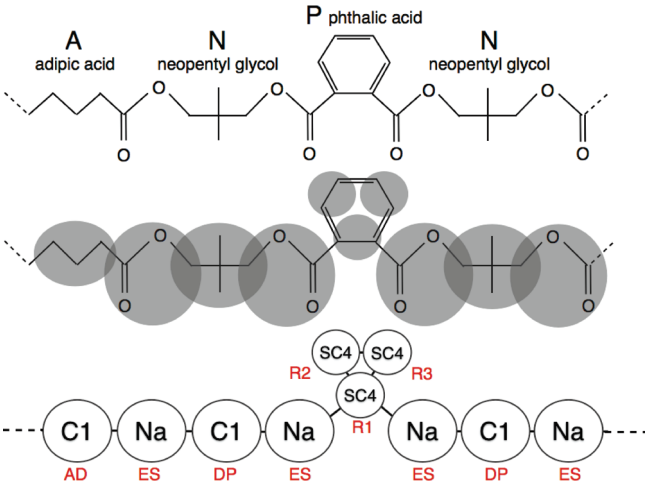

Figure 2. Atomistic-to-CG mapping schemes. Na, C1, and SC4 are MARTINI bead types.[15] AD, ES, DP, R1, R2, and R3 are the bead names used in this work.

Table 1. Parameters for the Harmonic Functions Describing Bond and Angle Interactions[a]

bond	l_{eq} [nm]	k_b [kJ/mol nm^2]
AD−ES	0.365	6000
ES−DP	0.33	8000
ES−R1	0.26	8000
R1−R2	0.27	constr.
angle	θ_{eq} [deg]	k_θ [kJ/mol rad^2]
ES−AD−ES	145	25
ES−DP−ES	130	45
DP−ES−R1	125	200
ES−R1−ES	94	300
ES−R1−R2	105	400
AD−ES−DP	125	25

[a] Bead names, not to be confused with MARTINI bead types, are the same as in Figure 2. R2−R3 and R3−R1 bonds are constrained to the same value as R1−R2. Analogously, the ES−R1−R2 angle parameterization holds also for the ES−R1−R3 angle.

We used standard mapping of MARTINI bead types whenever the building blocks were the same as in the original MARTINI force-field (see Table 3 in the paper by Marrink et al.[15]). In the case of building blocks never used before, the initial choice of the bead type was based on chemical similarity and then validated by comparing calculated thermodynamic properties with experimental data.

Figure 2 illustrates the mapping we have chosen. The ester functional group is represented in MARTINI by the Na bead type. Each Na bead was mapped onto the center of mass of the $-COOCH_2-$ group, the CH_2 group being weighted 1/2 in order to be shared with the neighboring neopentyl glycol bead. The 4-carbon alkyl chain in adipic acid can be represented by a C1 bead in MARTINI. The same C1 bead can be used for neopentyl glycol, provided that the two external backbone C atoms are shared with the adjacent ester beads. The pendant ring of phthalic acid can be represented by three interconnected SC4 beads, like benzene in the original MARTINI parametrization. Since the same MARTINI type can represent different chemical moieties, we refer to the beads using the bead names reported in Figure 2.

Bonded Interaction Parameters. Consistently with the MARTINI scheme, we described bonded interactions in the CG model by means of simple harmonic bond and angle potentials. For the sake of simplicity, we did not include any torsional angle at the CG level, a strategy already adopted in the development of the polystyrene model.[13] The optimization of equilibrium values and elastic constants for bond lengths and angles relied on bond and angle distributions obtained from atomistic simulations. Details about the choice of atomistic force-field parameters, which were taken from OPLS-AA,[33,34] can be found in the Supporting Information. Atomistic simulations were performed by means of the GROMACS 4.0.2 MD package, in the NpT ensemble with temperature and pressure controlled by the Nosé−Hoover and Parrinello−Rahman thermostat and barostat, respectively. Time step was set to 2 fs. A system containing 125 AN and 125 PN dimers was equilibrated at room temperature and atmospheric pressure. The distributions of bonds and angles connecting the centers of mass of the groups of atoms to be mapped onto the CG description were averaged over 200 ns trajectories.

Equilibrium values for CG bonds and angles were chosen as the average value of atomistic distributions. CG force constants were tuned to reproduce the width of the atomistic distributions. CG simulations for the optimization of bonded interactions were run in the same ensemble and thermodynamic conditions as the atomistic simulations, with a time step of 20 fs. Table 1 contains the equilibrium values and elastic constants for all the bonded interactions in the CG polyester chains.

Nonbonded Interaction Parameters. Nonbonded interactions between neutral beads in MARTINI are described by Lennard-Jones functions. The strength of the interaction, ε, is optimized based on experimental thermodynamic data. In the MARTINI force field, beads have the same size and mass when they represent four heavy (non-hydrogen) atoms (four-to-one mapping). Beads with smaller size and mass were introduced[15] to better match the structure of cyclic compounds, such as benzene and cyclohexane (represented by three interconnected small beads). Smaller beads are used when the mapping is two-to-one. A further reduction of some of the beads' size proved to be useful in the case of the CG model of polystyrene,[13] and allowed for a better reproduction of experimental density and radius of gyration in the melt.

According to the mapping we chose, a two-to-one mapping holds for R1, R2, and R3 beads. These should therefore be represented by small beads. A four-to-one mapping holds for AD and DP beads, so the choice of large beads is again straightforward. A three-to-one mapping holds for ES beads, therefore posing the problem of choosing between large and small size. To validate the choice of bead sizes for the ester moiety, we calculated the density of a solution of AN and PN dimers (50% of each species) in atomistic simulations and in coarse-grained simulations using either Na or SNa for the ester group. In all-atom simulations at room temperature and atmospheric pressure, we obtained a density ρ_{atom} = 1076 kg/m^3. In CG simulations, the better agreement was given by the topology containing large beads (Na), for which the density of the mixture was 1047 kg/m^3. The optimal choice of bead types for our polyester chain is thus the one shown at the bottom of Figure 2.

Coarse-Grained Model of the Cross-Linking Agent. A common cross-linking agent for polyester-based steel coatings is hexa(methoxymethyl)melamine (HMMM), shown in Figure 3. Polyester/HMMM coatings dominate the market due to their

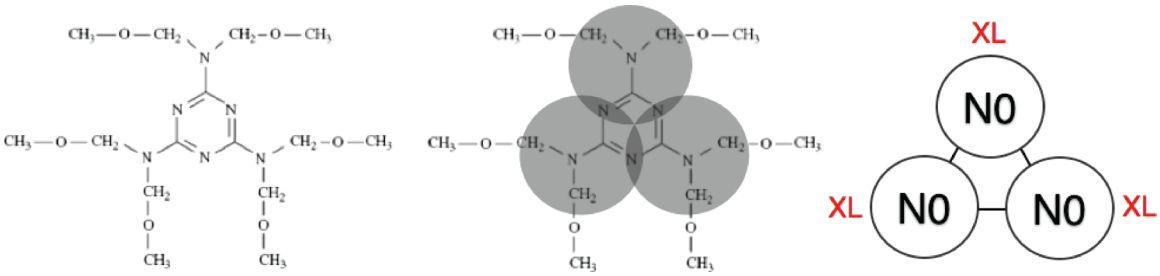

Figure 3. Atomistic-to-CG mapping scheme for the HMMM molecule. N0 is the MARTINI bead type,[15] XL is the bead name used in this work.

high performance in formability, scuff resistance, durability, and cost effectiveness.[35] During cure, the melamine methoxy groups react with the polyester hydroxyl groups, resulting in the loss of methanol. Typical peak temperatures of the steel substrate during cure are around 500 K. Self-condensation of melamine can take place during cure,[35] as well. An excess of self-condensation of the cross-linker results in poorer mechanical performance of the coating.[36]

Mapping and Bonded Interactions. In analogy with the treatment of ring molecules by MARTINI, we mapped the HMMM molecule using three beads (corresponding to a five-to-one mapping, as shown in Figure 3). We placed each CG bead at the center of mass of two (CH_2) groups, an N atom, and a C and two N atoms from the triazine ring, the latter N atoms being shared with neighbor beads. Because of the stiffness of the molecule, we constrained the distance between the melamine CG beads at its equilibrium value of 0.4 nm.

Nonbonded Interactions. We chose the particle type for HMMM beads based on the free energy of transfer of the entire HMMM molecule between water and octanol. According to Klimisch et al.,[37] the experimental partition coefficient of HMMM between water and octanol is log P_{ow} = 1.61. This corresponds to a Gibbs free energy of transfer of ΔG_{wo} = 9.3 kJ/mol. By thermodynamic integration (TI, calculation details can be found in the Supporting Information) we evaluated the free energy difference of candidate triangular molecules built with different MARTINI types (with large and intermediate polarity), and found that the molecule composed of three N0 type beads provides the best agreement to the experimental data, with ΔG_{wo} = 11.4 kJ/mol (the more polar Na bead yields ΔG_{wo} = 6.6 kJ/mol).

Cross-Linking Interactions. Cross-links are covalent bonds formed between the terminal hydroxyl groups of the polymer chains and the HMMM methoxy groups. Self-condensation of melamine, namely the formation of HMMM−HMMM bonds, is a common side reaction. We have modeled the formation of cross-links by introducing an *ad hoc* potential between the HMMM beads (named XL) and some of the terminal beads of the chains (named CE), and between XL and XL beads. The *ad hoc* potential is harmonic at distances shorter than 0.5 nm, and it is smoothly switched to 0 kJ/mol between 0.5 and 0.6 nm by means of a fourth-order polynomial. The elastic constant in the harmonic part is the same as in the backbone bonds ES-DP (k_b = 8000 kJ/mol), and has a minimum at 1_{eq} = 0.4 nm.

As melamine diffuses through the polymer melt, bonds are formed between XL beads and CE beads when their reciprocal distance becomes short enough. This is similar to what has been done in previous MD simulations of cross-linked networks.[23,32] The well of the potential is deep enough as to prevent the cross-links from breaking during simulations at the temperatures of interests (T < 600 K). The degree of cross-linking is tuned by choosing *a priori* how many terminal beads will interact with XL beads via the cross-linking potential (the simulation time always allows for more than 98% of the reactive chain ends to be cross-linked).

Simulation Protocols. *Systems.* Our reference system is composed of polyester chains with a 3:7 adipic:phthalic acid content by weight. This adipic:phthalic acid ratio is the same as the one used during the synthesis of the experimental samples described in the section Experimental Methods. The molecular mass of the chains in the samples provided by Becker Industrial Coatings Ltd. (BIC) is widely distributed, with a maximum at M_w = 8400 amu. In our simulations, we considered monodispersed systems of chains with 60 monomers each. Assuming a 3:7 adipic:phthalic acid content, this chain length corresponds to M_w = 8100 amu. We assumed that the resin has no tendency to form diblock configurations (where AN and PN dimers phase separate along the polymer chain) during the synthesis stage. This assumption is supported by experimental data, as better detailed in the Results section. As a consequence, we randomized the position of AN and PN dimers along the chains.

All simulations were performed on systems comprising 48 polyester chains. We considered three different samples: a noncross-linked sample, a partially cross-linked sample, and a fully cross-linked sample. The two cross-linked samples contain 60 HMMM molecules, corresponding to a 5% loading. In the partially cross-linked sample, only one of the two ends of each polyester chain is allowed to react with HMMM molecules via the harmonic cross-linking potential. In the fully cross-linked sample, all chain ends are reactive.

All CG molecular dynamics simulations described in the following were run in the NpT ensemble, with a time step of 20 fs, as detailed in the Supporting Information.

Pure Resin Melt Equilibration. First, 48 chains were stacked close to each other in an intermediate-coiled state, and allowed to collapse at T = 500 K into a melt with homogeneous density. After stacking and collapsing, melts were equilibrated at T = 500 K for a period of time Δt_{eq} = 1 μs. The self-diffusion coefficient of the chains of the reference system during equilibration was measured as $D = 1.2 \times 10^{-8}$ cm^2/s, and the chains could diffuse over a length scale comparable to their radius of gyration in 0.3 μs. Starting from the equilibrated snapshot, at least 11 independent equilibration runs of 0.3 μs were performed. The equilibrium density for the samples is 1300 kg/m^3, which reasonably compares to the density of the largely polydisperse experimental samples, 1110 kg/m^3. For the characterization of the mechanical properties of the noncross-linked resin, each final equilibrium configuration was cooled down to 300 K at the rate of 1.25 K/ns. Snapshots from the cooling simulations were used as starting configurations

for the tensile simulations of the noncross-linked systems, as described in the Tensile Tests paragraph below.

Cross-Linking. First, 60 HMMM molecules were inserted, at random positions, in each of the independent equilibrium configurations generated at T = 500 K. After removing possible overlaps by local energy minimization, the system was equilibrated for Δt_{eq-x} = 0.1 μs at T = 500 K. We remark here that during Δt_{eq-x}, cross-links (XL−XL and XL−CE bonds) were not activated. The aim of performing such a high-temperature equilibration was to allow for a proper dispersion of the HMMM molecules into the resin. During paint preparation, the dispersion of the cross-linking agent takes place at room temperature, but it is favored by the presence of solvents, which are not included in our model. In our simulations at T = 500 K, HMMM molecules diffused in the reference system with a diffusion coefficient $D_{HMMM} = 8.0 \times 10^{-7}$ cm^2/s, thus moving over the whole simulation box during Δt_{eq-x}.

After dispersion, all the XL−XL bonds and all (or half of) the XL−CE bonds were activated during a run of 0.1 μs at T = 500 K. This simulation time allowed for the formation of more than 98% reactions between the active chain ends and the cross-linkers, consistently with what reported in the MD work by Heine et al.[23] The cross-linked network was subsequently cooled down to 300 K at a rate of 1.25 K/ns. The equilibrated and cooled cross-linked configurations were then transferred to the tensile test stage.

Tensile Tests. Tensile tests are performed by applying a semi-isotropic pressure coupling to the simulation box. The p_{XX} and p_{yy} stress tensor components were set to atmospheric pressure, while the system compressibility was set to 0 along the z direction. The z edge of the simulation box was then expanded at the constant displacement rate of 8.3×10^{-8} nm/ps, corresponding to a strain rate, in the elastic regime, of 1.32×10^4 s^{-1}. The box expanded in the z direction until its z edge was enlarged by 1.2%. After averaging the stress−strain curves resulting from at least 11 independent runs, values of Young's modulus (E) were obtained as the slope of the best linear fit of the stress−strain curves in the 0−1% strain range.

EXPERIMENTAL METHODS

Materials and Sample Preparation. The paint formulation was prepared in the facilities of Becker Industrial Coatings, U.K.. The polyester resin, the hexa(methoxymethyl)melamine (weight ratio HMMM: resin = 20:80 in the solid film) as well as two different solvents and a flow agent (all of which are assumed to evaporate completely during cure) were added one by one and mixed for 30 min with an electric stirrer. Subsequently the paint was applied on polytetrafluoroethylene-coated steel panels with the use of a No. 30 draw-down bar. The paint was then cured inside an air oven for 30 s at 538 K to a peak metal temperature of 505 K. The panels were subsequently placed for a few seconds on a magnetic plate to cool and were stored at room temperature.

Free films of the coatings, 25 μm thick, were then removed from the panels and samples were cut to the desired dimensions with a razor blade. For tensile testing, rectangular samples were cut from films with dimensions 6 mm × 60 mm. Paper end-tabs were bonded on the samples with the use of a commercial cyanoacrylate adhesive, leaving a sample free-length of 40 mm. The use of end-tabs was necessary to improve the grip of the samples inside the tensile clamps. For DMA, rectangular samples were prepared with a width of 5 mm and a length of about 15 mm (samples were made significantly longer than the fixed 5 mm distance between the DMA tensile grips in order to make clamping easier.) The use of end-tabs for DMA samples was not required as there was no observed slippage during testing.

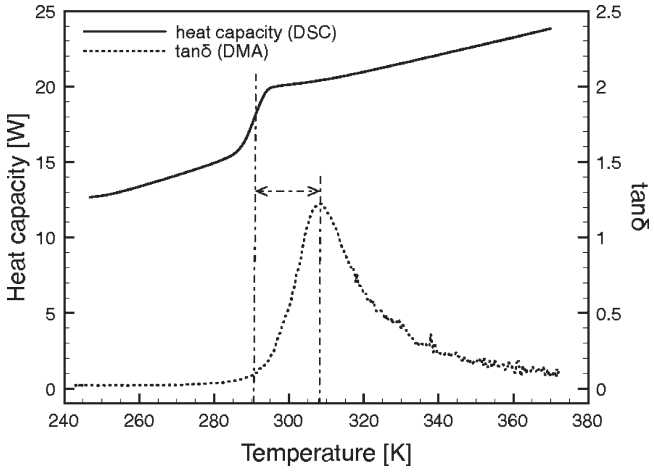

Figure 4. Experimental measure of the glass transition temperature of the HMMM-cross-linked polyester resin: heat capacity vs temperature data from DSC and tan δ values from DMA.

Experimental Procedure. Differential scanning calorimetry (DSC) was employed to measure the glass transition temperature (T_g) of the paint. About 10 mg of the cured sample were tested in two heating cycles over a temperature range between 243 and 373 K at a rate of 10 K/min with the use of a Q2000 DSC (TA Instruments, UK). T_g was measured as the midpoint of the transition region on the heat flow versus temperature curve, according to the specifications from the British Standards Institution (BSI) standard BS 11357−2.[38]

For tensile tests, samples were loaded to failure (see BS 527−3 and BS 527−1[39,40]), at a displacement rate of 5 mm/min with the use of an Instron 4301 universal testing machine with a 100 N load cell. This displacement rate corresponds to an initial strain rate of about 2×10^{-3} s^{-1} for a sample free length of 40 mm. The effect of moisture on the mechanical properties of thin polymeric films has been clearly demonstrated in the literature[41,42] and, for the purpose of this study, all tests were performed under a constant relative humidity of 50%. Tests were conducted at different temperatures ranging between −30 and +30 K from T_g, inside an environmental chamber that provided both temperature and relative humidity control. An equilibration period of 10 min in the chamber was allowed for all samples before testing.

For dynamic mechanical analysis, samples were tested in tensile mode at a frequency of 1 Hz with the use of a Tritec 2000 dynamic mechanical analyzer (Triton Technology Ltd., U.K.). The distance between the DMA clamps was set to 5 mm and an amplitude of 8−10 μm was chosen, corresponding to 0.16 to 0.2% strain. As a result, a strain rate of 0.3 to 0.4% per second was obtained. Because of the low stiffness of the samples it was necessary (see Gabbot[43] for a discussion of DMA testing of thin films) to apply a static tensile load of 0.5 N at the beginning of the test to prevent buckling. As the stiffness of the sample decreased, the DMA machine automatically adjusted the preload to smaller values to ensure that the material properties remained within the linear viscoelastic region. No control of relative humidity was possible, and samples were tested over a temperature range between 253 and 373 K at a rate of 3 K/min.

RESULTS

Experimental Characterization. *Glass Transition.* Figure 4 reports the specific heat vs temperature curve as measured by DSC. The glass transition temperature of the coating, T_g, is 291 K (midpoint) with onset and end temperatures at 287 and 294 K, respectively.

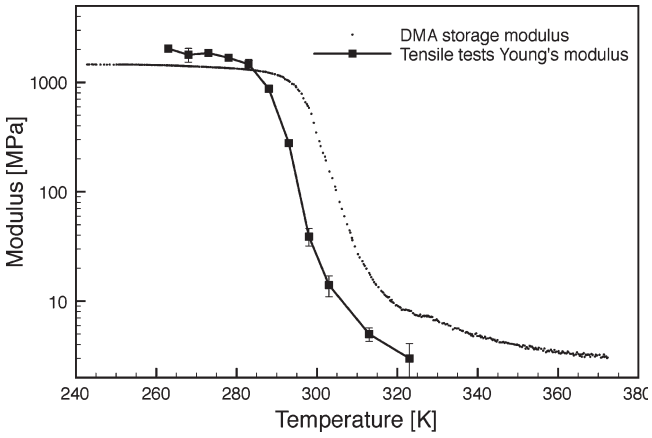

Figure 5. Young's modulus and the storage modulus of the polyester−HMMM coating.

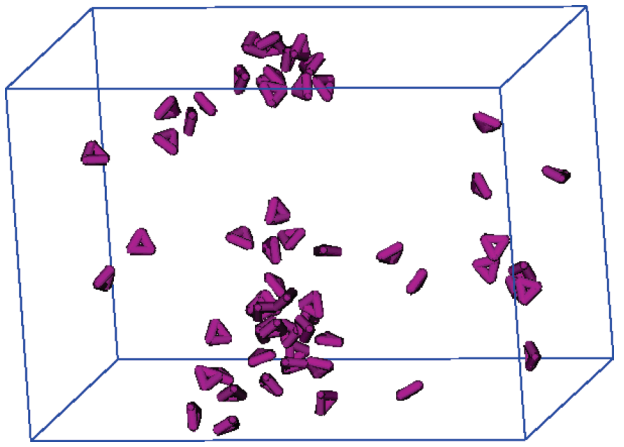

Figure 6. Melamine molecules, represented by triangles, during the equilibration of the resin−HMMM system at 500 K. The resin beads are not shown for clarity. The reaction between HMMM molecules and the terminal beads of chains is not activated here, but HMMM molecules tend to form metastable aggregates.

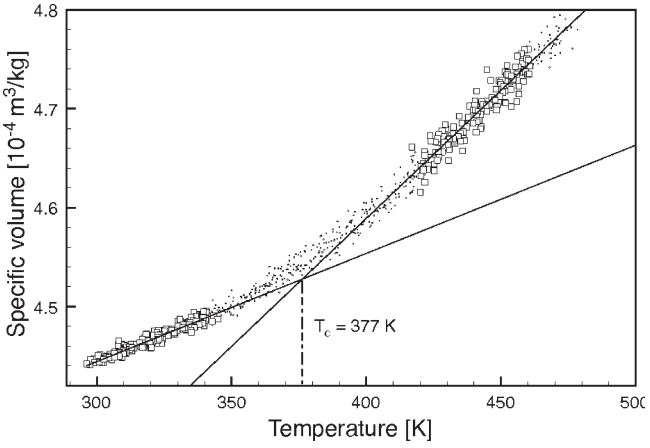

Figure 7. Estimate of the critical temperature T_c for the liquid to glass transition of the partially cross-linked system. Temperature ranges for fitting are 300−340 K for the glassy phase and 420−460 K for the liquid phase, as highlighted by square symbols.

The glass transition temperature was also determined by DMA. In DMA, an oscillating strain is applied to the sample. The resultant oscillating stress and its phase angle difference, δ, with respect to the applied strain are recorded as outputs. The temperature corresponding to the peak of the tan δ curve is often used as a measure of the glass transition temperature of polymers.[1,44] Here this was found to be 307 K. No secondary peaks can be observed, coherent with the hypothesis that the sample does not contain diblock (AN−AN−AN−...−PN−PN−PN) structures. Clearly the glass transition temperature as measured by DMA is much higher than the corresponding DSC value. Indeed differences in the order of 10−20 K between the two methods have been reported,[44] and therefore, the agreement between DMA and DSC data presented here is considered satisfactory.

Tensile Tests. The Young's modulus was calculated as the slope of the stress vs strain curves in the linear region (between approximately 0.2 and 0.8% strain). In Figure 5 the results are shown for different temperatures. Two regions are clearly observed in the figure. At low temperatures the coating behaves in a glassy manner returning modulus values between 1.5 and 2 GPa. At approximately 5 K below T_g, the modulus starts to drop significantly reaching about 4 MPa at $T - T_g = +32$ K. The onset of the transition region on the modulus plot agrees well with the observed onset from DSC data.

In Figure 5, we plot also the values of the storage modulus acquired by DMA. Tensile and storage moduli are two different material properties, but still they are expected to exhibit a significant degree of agreement. This is indeed the case here. We found that the tensile modulus curve is shifted to the left of the storage modulus. We hypothesize that this is due to a combination of factors: the different strain rates applied in tensile tests and DMA; the fact that tensile tests were carried out under temperature equilibrium whereas DMA samples were subjected to a temperature ramp with a resultant effect of thermal inertia; and, perhaps more importantly, the 50% relative humidity conditions at which tensile tests were performed.

MD Simulations. *Structure.* From the simulation of the pure, non-cross-linked resin melt, at a temperature of 500 K, our reference system is found to have a persistence length of 0.54 ± 0.01 nm. To our knowledge, no experimental data are available for a direct comparison. Atomistic simulations[45,46] performed on similar polyesters indicate that their persistence length varies in the 5−9 Å range. The root-mean-square radius of gyration of the chains at equilibrium is $R_g = 2.3 \pm 0.1$ nm, while the ratio between the mean square end-to-end distance and the mean square radius of gyration is 6.01 ± 0.5 nm, consistent with Gaussian chain statistics.[47]

Before the activation of cross-links, HMMM diffuses through the simulation box showing some tendency to form aggregates, as shown in Figure 6.

Thermodynamics. Upon insertion of the cross-linking agent and activation of the cross-linking interactions, the dynamics of the system is strongly suppressed and an increase in the glass transition temperature is expected. In order to identify the transition of the noncross-linked, partially cross-linked and fully cross-linked samples, we collected the specific volume, v, vs temperature while cooling at the rate of 1.25 K/ns. The data in the liquid (420−460 K) and solid (300−340 K) temperature ranges were fitted by linear functions $v = a_s T$ and $v = a_l T$, where a_l and a_s represent the thermal expansion coefficients in the two phases. The temperature at which the linear functions meet is a critical temperature T_c for the transition from the rubbery to the glassy state. Data for the partially cross-linked sample, resulting from 11 independent cooling simulations, are shown in Figure 7.

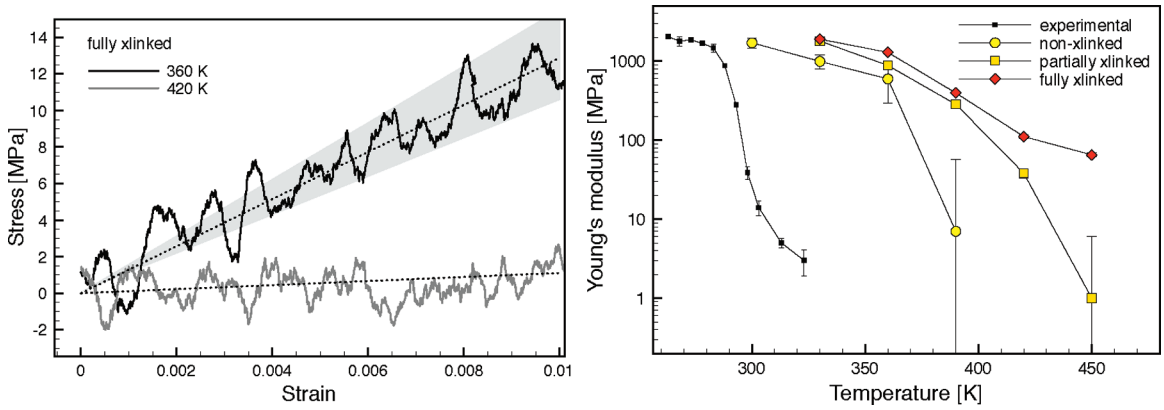

Figure 8. On the left, stress−strain curves obtained from the *in silico* tensile tests performed on the fully cross-linked sample, at 360 and 420 K. Dashed lines are the linear fit curves used to estimate E values. For the data at 360 K, the linear fit curves delimiting the gray area have been used to estimate the error bar on the E values. This procedure was repeated on all sets of data (see right panel). On the right, Young's moduli plotted as a function of temperature. Where the error bars are not visible, they are smaller than the symbols used.

Here, T_c was found to be 377 K. Using the same analysis we found a value of 355 and 392 K for the T_c of the noncross-linked and fully cross-linked systems, respectively.

Tensile Tests. In Figure 8, left panel, two exemplary stress−strain curves and their linear fit curves are shown. They refer to the fully cross-linked sample, at the temperatures of 360 and 420 K. The Young's modulus, E, corresponds to the slope of the linear fit curves in the 0−0.01 strain range. The right panel of Figure 8 reports the values[68] of the Young's modulus vs temperature, for the non-cross-linked, partially cross-linked, and fully cross-linked systems.

The moduli of the non-cross-linked system have values in the 1−2 GPa range in the solid phase and remain lower than the moduli of the cross-linked systems throughout the temperature range considered. The values of E for the two cross-linked samples coincide at 330 K (2 − 2.5 GPa), which is well below glass transition. In the glass transition region, the Young's modulus of the partially HMMM-cross-linked system decreases to 1 MPa at 450 K. As for the fully cross-linked sample, the Young's modulus drop is much less pronounced, with E close to 100 MPa at 450 K.

The glass transition of the noncross-linked and partially cross-linked systems, associated with a drop of *E* by more than 1 order of magnitude, are in agreement with the critical temperatures for the glass transition derived from specific volume plots (see Figure 7).

DISCUSSION

We highlight here the main differences between the real samples and their *in silico* counterparts. The resin samples used in this work have a polydispersity index of 2.2 (defined, as usual, as the ratio between the weight-average molecular weight, and the number-average molecular weight), while our simulations have been performed on monodispersed samples. Qualitatively, the width of the distribution of molecular weights in the resin is expected to affect the distribution of chain lengths between cross-links. The broader the distribution, the wider the glass transition, typically resulting in a better impact resistance.[1]

The second important difference between the real and the *in silico* samples compared in this paper is the concentration of the cross-linker agent. The solid weight ratio of 20:80 HMMM: polyester characterizing the samples used in the experimental part of this work is consistent with the typical concentrations used during the preparation of the paints.[35] Still, such a concentration is much higher than the stoichiometric concentration required to cross-link the sample (approximately 1.8 wt % in the solid film). The reason for the use of excess HMMM is related to its tendency toward self-condensation, effectively resulting in a decrease of its functionality. The use of such a high concentration of HMMM is empirically known to provide a satisfactory degree of cross-linking to the system but, at the same time, micrometer sized HMMM aggregates can be formed in the coating.[48] Modeling the effects of these large HMMM aggregates on the mechanical properties of the coating can not be addressed by state-of-the-art MD simulations. We have thus reduced the HMMM content in the *in silico* sample, aiming at a faithful description of the coating properties far from the high-HMMM concentration regions.

Glass Transition. We have located the range of temperatures where the system undergoes its glass transition by means of computational and experimental tools. The results from cooling simulations and simulated tensile tests agree reasonably well. The signatures of the solid to liquid transition as located by our cooling simulations are located at 355, 377, and 392 K for the noncross-linked, partially and fully cross-linked sample, respectively. In simulated tensile tests, the Young's modulus drop takes place in the 350−370, 360−380, and 390−420 K ranges, respectively. Cooling and strain rates in our simulations, though, are much faster than the heating and strain rates used in DSC and experimental tensile tests. On the basis of the time−temperature superposition principle,[49] we can quantitatively estimate at which temperature the experimental samples would undergo the glass transition, if they were strained (or cooled) at the same strain (or cooling) rate used in simulations. By comparing the resulting shifted transition temperature with the one we obtain in simulations, we can test the reliability of the model. As tensile tests *in silico* and in the laboratory have been performed according to very similar protocols, we use the ratio of our experimental and computational strain rates to provide an estimate of the shift of the glass transition temperature of the real sample, when deformed at the fast strain rate we used in simulations.

Using multiple frequency DMA data, a master-plot of the storage modulus over a wide range of times can be obtained. To achieve this, a sample was tested using DMA at 3 different frequencies (0.1, 1, and 10 Hz) while, at the same time, the temperature

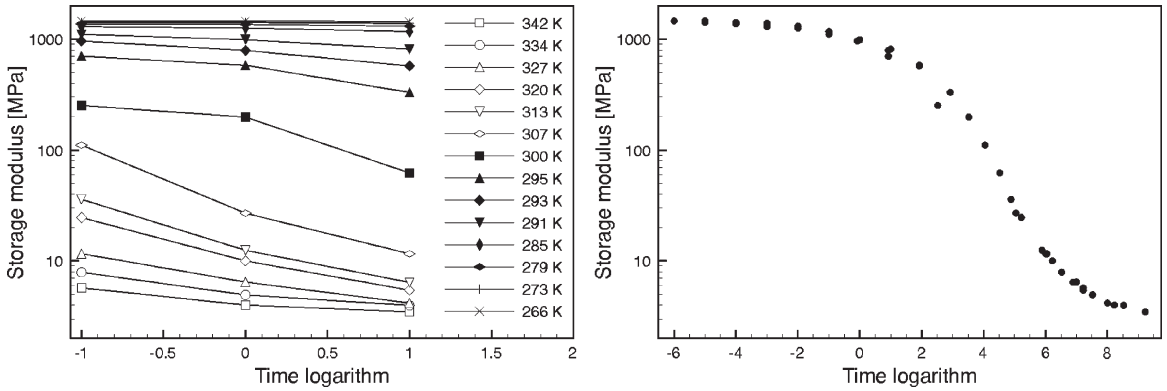

Figure 9. Left: isotherms of the storage modulus. Right: storage modulus master curve. Time units used are seconds.

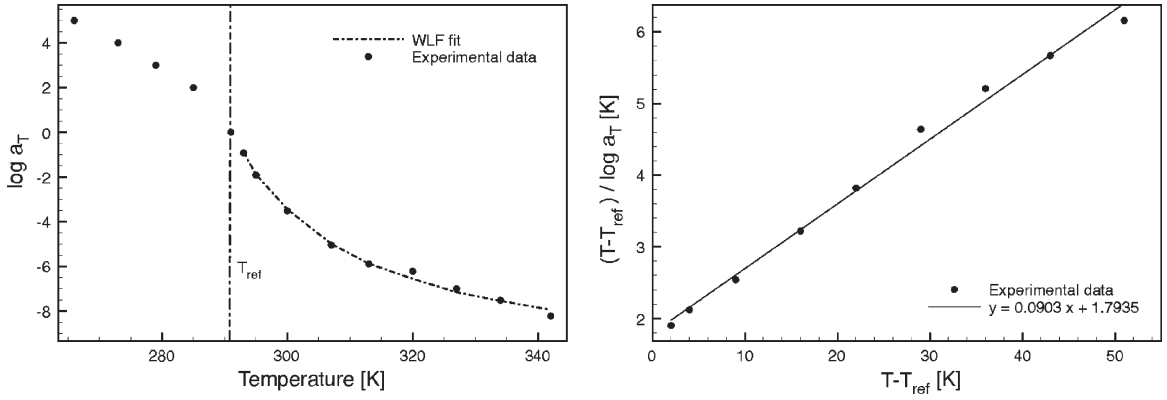

Figure 10. Shift factors plotted as a function of temperature. The dashed line represents the best fit to a WLF behavior, as obtained from the linear fit on the right.

was increased at a rate of 2 K/min from 253 to 373 K. As a result, values of storage modulus corresponding to the material response under frequencies of 0.1, 1, and 10 Hz could be obtained at all temperatures within the temperature range of the test. By taking the inverse of frequency, the time required for the sample to go through one cycle of strain was obtained. In Figure 9 (left), the isotherms of the storage modulus are plotted against the logarithm of the time required to complete one strain-cycle.

These isotherms can then be shifted along the time axis with respect to a reference temperature to produce a single curve of storage modulus versus time. In this case, the reference temperature was chosen as 291 K, which is the T_g of the formulation as measured by DSC and corresponds to the steep drop of the Young's modulus in the experimental tensile tests. Therefore, the isotherm at 291 K was kept at its original position, while the rest of the isotherms were shifted to either shorter or longer times until a good overlap of storage modulus values was achieved. The validity of this approach is based on the assumption that the material is thermo-rheologically simple (for a review on thermo-rheological simplicity see Plazek[50]). Our superposition of the isotherms results in a smooth master curve, as shown in Figure 9 (right), which supports the validity of time−temperature superposition for the material used in this study.

The distance by which each isotherm is shifted along the time axis to create the storage modulus master curve is called the shift factor of this particular isotherm. The shift factors used for the construction of the storage modulus master-curve are plotted versus temperature in Figure 10. Two regions can be observed in the shape of the log a_T vs T plot. Up to temperatures of approximately 295 K, the graph can be approximated by a straight line, and the polymer behavior can be described by an Arrhenius type relationship. At higher temperatures, the points deviate from linearity substantially, and the empirical Williams−Landel−Ferry[51,52] (WLF) equation is more suitable to describe the large scale intermolecular dynamics:

$$\log(a_T) = -\frac{C_1(T - T_{ref})}{C_2 + (T - T_{ref})} \quad (1)$$

where a_T is the shift factor at temperature T, T_{ref} is the reference temperature usually taken as the T_g and C_1 and C_2 are material-dependent constants. For temperatures above T_g, a linear fit of $(T - T_{ref})/[\log a_T]$ plotted versus $(T - T_{ref})$ allows the determination of the WLF constants C_1 and C_2. Figure 10 shows our fit, from which the WLF constants were determined as $C_1 = 11.03$ and $C_2 = 19.65$.

On the basis of the knowledge of WLF constants, and of the time shift factor between the experimental and *in silico* strain rates used during our tensile tests, we can estimate the reliability of the model in locating the glass transition temperature of the system. We have to point out that, both in experimental and simulated tensile tests, our procedures allow for the control of the displacement rate, and not of the strain rate. Still, if we limit our comparison to small strains, in the elastic regime, we can safely neglect the difference. The experimental strain rate is thus $r_{exp} = 2 \times 10^{-3}\ s^{-1}$, and the one used in simulations is $r_{sim} = 1.32 \times 10^{4}\ s^{-1}$,

dx.doi.org/10.1021/ma200788a |*Macromolecules* 2011, 44, 6198–6208

giving $a_T = r_{exp}/r_{sim} = 1.5 \times 10^{-7}$. Equation 1 can be rewritten as:

$$T - T_{ref} = -\frac{\frac{C_2}{C_1}\log(a_T)}{1 + \frac{\log(a_T)}{C_1}} \quad (2)$$

As a reference temperature, we choose again T_{ref} = 291 K. $T - T_{ref}$ is thus the temperature shift expected by the WLF equation for a sample stretched at the strain rate used in simulations, and it results as $T - T_{ref}$ = 31 K.

Such a shift does not account for the whole >60 K shift that results from the comparison of the E onset values from tensile data, even taking into account the uncertainty related to the actual degree of cross-linking of the experimental sample. Another factor affecting the glass transition temperature of the coating is the relative humidity. Foster et al.[41] have reported about the effect of moisture on the mechanical performances of a thermoset polyester resin, similar to the one analyzed in our paper. The glass transition temperature can decrease by 10 K when going from 20 to 80% relative humidity. All the experimental measurements reported in the paper have been conducted at a relative humidity of 50%, while no water molecules are ever considered in our computer simulations. Humidity could thus contribute to reduce the gap between the T_g measured experimentally and the one obtained *in silico*.

Eventually, differences between the T_g of the model and of the experimental samples are not surprising, as the degree of accuracy of coarse-grained models in capturing liquid−solid transitions is not expected to be very high. For MARTINI-based force-fields, in particular, the enhanced stability of the solid phase at the expense of the liquid one is a known limitation of the model.[15] We consider that the location of the T_g with an accuracy of 10−15% is satisfying, and nevertheless invite users to deal with this point with the necessary caution.

Concerning the effect of the degree of cross-linking on the glass transition temperature of the coating, we can state, based on Beckers' experience, that the T_g of polyester coatings is usually observed to be shifted upward by 15−20 K as an effect of curing. These data are consistent with the temperature shifts obtained from our simulations.

Tensile Tests. In the glassy phase, at low temperature, the value of the Young's modulus measured by our simulated tensile tests is in very good agreement with the experimental values. In general, reliable compressibility values result from the use of the structure-based coarse-grained models, such as inverse Monte Carlo[53] and iterative Boltzmann inversion[54] models, where the radial distribution functions (RDFs) at the CG level reproduce with large accuracy those obtained in atomistic simulations. MARTINI, at variance with the above-mentioned structure-based potentials, does not take into explicit account the RDFs during its parametrization procedure. Still, the fact that our Young's modulus values are in such good agreement with the experimental values can be assumed as an indirect proof of its reliability in reproducing the structural properties of the melt.

Another factor that can affect the mechanical properties is the dynamics at CG level. Coarse-graining is known, in general, to accelerate the system dynamics (diffusion and relaxation processes), thus favoring the appearance of small plastic deformations within the elastic stress−strain regime .[2,55] The extent to which the dynamics is accelerated depends on the degree of coarse-graining.[56] Coarse-grained models of polystyrene (PS) are a valid example. In models where each PS monomer is represented by a single bead, the chain dynamics is much faster than that of PS in atomistic simulations (independent studies[57,58] report acceleration factors of several hundreds). We recently developed a MARTINI model of PS that is based on a finer degree of coarse-graining. In this model, each monomer is represented by four beads and the backbone-ring structure of PS is retained at the coarse-grained level. At variance with the more coarsened models, the dynamics of our MARTINI model appear to be only 2−4 times faster than in atomistic simulations.[13] We do expect a similar dynamics acceleration in our polyester system, based on the similarities between the two models. Moreover, MARTINI has been proven to be reliable in reproducing the Young's and bending modulus of other systems, such as proteins[59] and membranes.[15,20]

The E vs T trends shown in Figure 8 are shifted to higher temperatures when going from the noncross-linked to the partially and fully cross-linked samples. These temperature shifts are consistent with the different temperatures associated with the glass transitions of the three samples (see previous paragraph). Moreover, our simulations allow for an estimate of the effect of cross-linking on the elastic response of the sample. The modulus drop takes place over a larger and larger temperature range as the degree of cross-linking increases. This result is consistent with the current knowledge about the effect of cross-linking on the glass transition of polymer systems. Such a broadening effect has been reported in a number of publications[60−62] that examine the dielectric relaxation spectra of polymers with different degrees of cross-linking. Roland[62] related high cross-link densities to an increase in intermolecular cooperativity, resulting in a broader distribution of the relaxation spectra (for a discussion on intermolecular cooperativity and its effects on relaxation spectra see also[63]). More recently, similar conclusions were drawn from the examination of dynamic mechanical data.[64]

The model thus appears to capture correctly the broadening effect of cross-linking on the glass transition of the polyester resin. Nevertheless, some discrepancies with the experimental data have to be highlighted here. In general, different mechanisms can affect the broadness of the glass transition. First, as noted above, a higher degree of cross-linking corresponds to a broader transition. Second, the wider the molecular weight distribution, the broader the transition.[65−67] Let us now compare the E vs T trend of the experimental sample, with that of the noncross-linked *in silico* sample. Both the above-mentioned mechanisms would lead us to expect, for the cross-linked and polydispersed experimental sample, a broader transition than for the noncross-linked, monodisperse *in silico* sample. In Figure 5, instead, the transition of the two samples looks comparable, if not broader for the *in silico* sample. We speculate that a possible reason for this difference is the limited size of the *in silico* sample, which does not allow us to capture the structural and dynamical heterogeneity of the real sample. This issue warrants future investigations.

■ CONCLUSIONS

In this paper, we have derived a coarse-grained model of a typical thermoset polyester coating with applications in the steel coating industry. The model parametrization is based on the MARTINI[14−16] force-field, originally developed for molecules of biological interest and recently applied to the study of polymers.[13,21] When used in molecular dynamics simulations, our coarse-grained model is faster than its all- or united-atom counterparts by at least a factor of 40, due to a 4-to-1 reduction of the

number of particles and the use of a 20 fs time step. A further speed-up of 2.5 is due to the fact that no long-range Coulomb interactions are computed, resulting in a total speed-up factor of 200 at least. We designed our model and simulation protocols in such a way as to include the formation of cross-links between the polyester molecules and a hardener added to the resin. One of the main strengths of the model is its ability to deal with such a complex, multicomponent system and still to retain the system's important chemical specificity. In order to demonstrate this point, we have compared our simulation outcomes to the results of the experimental characterization of the coating. We have performed *in silico* and experimental tests concerning the thermodynamic and mechanical properties of the system. The model turns out to locate with reasonable accuracy the glass transition of the system. Moreover, it is able to predict variations in the elastic response of the coating as a function of its degree of cross-linking.

We plan to develop our work in several directions. The computational advantages of our coarse-grained approach allow for the study of large samples, which could be made polydispersed so as to better mimic their experimental counterparts. As our MARTINI model includes relevant chemical details, we are currently studying how the chemical composition of the sample, and in particular, the relative concentrations of its acid components, affect its mechanical properties. Last but not least, we are investigating the mechanical reinforcement induced by the dispersion of nanofillers in the resin, which mutual interactions can be realistically captured by MARTINI. With a broader perspective, we expect that our coarse-graining approach will be applicable to a large variety of polymer systems, including those with direct applications at an industrial level.

■ ASSOCIATED CONTENT

Supporting Information. Atomistic simulations and coarse-grained simulations. This material is available free of charge via the Internet at http://pubs.acs.org.

■ AUTHOR INFORMATION

Corresponding Author
*E-mail: giulia.rossi@inserm.fr.

■ ACKNOWLEDGMENT

Authors from Aalto University and Tampere University of Technology acknowledge support by MatOx Ltd., by the Academy of Finland through its Center of Excellence COMP grant and by the research programme TransPoly. MatOx Ltd. acknowledges support by the Finnish Funding Agency for Technology and Innovation, TEKES. CSC IT Center for Science Ltd is acknowledged for the allocation of other computational resources. The authors acknowledge Bengt Ingman of Becker Industrial Coatings Ltd for useful discussions.

■ REFERENCES

(1) Wicks, Z. W.; Jones, F. N.; Pappas, S. P.; Wicks, D. A. *Organic Coatings: Science and Technology*, 3rd ed.; John Wiley & Sons, Inc.: New York, 2007.
(2) Fortunelli, A.; Geloni, C.; Lazzeri, A. *J. Chem. Phys.* **2004**, *121*, 4941.
(3) Hutnik, M.; Argon, A. S.; Suter, U. W. *Macromolecules* **1993**, *26*, 1097.
(4) Jang, S. S.; Jo, W. H. *J. Chem. Phys.* **1999**, *110*, 7524.
(5) Léonforte, F.; Tanguy, A.; Wittmer, J. P.; Barrat, J.-L. *Phys. Rev. Lett.* **2006**, *97*, 055501.
(6) Papakonstantopoulos, G. J.; Doxastakis, M.; Nealey, P. F.; Barrat, J.-L.; de Pablo, J. *J. Phys.Rev. E* **2007**, *75*, 031803.
(7) Kremer, K.; Grest, G. S. *J. Chem. Phys.* **1990**, *92*, 5057.
(8) Gersappe, D.; Robbins, M. O. *Europhys. Lett.* **1999**, *48*, 150.
(9) Baljon, A. R. C.; Robbins, M. O. *Macromolecules* **2001**, *34*, 4200.
(10) Lee, H.-N.; Rigglemand, R.; de Pablo, J. J.; Ediger, M. D. *Macromolecules* **2009**, *42*, 4328.
(11) Lee, H.-N.; Paeng, K.; Swallen, S. F.; Ediger, M. D. *Science* **2009**, *323*, 231.
(12) Riggleman, R. A.; Schweizer, K. S.; de Pablo, J. J. *Macromolecules* **2008**, *41*, 4969.
(13) Rossi, G.; Monticelli, L.; Puisto, S. R.; Vattulainen, I.; Ala-Nissila, T. *Soft Matt.* **2011**, *7*, 698.
(14) Marrink, S.-J.; de Vries, A. H.; Mark, A. E. *J. Phys. Chem. B* **2004**, *108*, 750.
(15) Marrink, S.-J.; Risselada, H. J.; Yefimov, S.; Tieleman, D. P.; de Vries, A. H. *J. Phys. Chem. B* **2007**, *111*, 7812.
(16) Monticelli, L.; Kandasamy, S. K.; Periole, X.; Larson, R. G.; Tieleman, D. P.; Marrink, S.-J. *J. Chem. Theory Comput.* **2008**, *4*, 819.
(17) Vuorela, T.; Catte, A.; Niemelä, P. S.; Hall, A.; Hyvönen, M. T.; Marrink, S. J.; Karttunen, M.; Vattulainen, I. *PLoS Comput. Biol.* **2010**, *6*, e1000964.
(18) Catte, A.; Vuorela, T.; Niemelä, P.; Murtola, T.; Segrest, J. P.; Marrink, S. J.; Karttunen, M.; Vattulainen, I. *Biophys. J.* **2008**, *94*, 983.
(19) López, C. A.; Rzepiela, A. J.; de Vries, A. H.; Dijkhuizen, L.; Hünenberger, P. H.; Marrink, S. J. *J. Chem. Theor. Chem* **2009**, *5*, 3195.
(20) Wong-ekkabut, J.; Baoukina, S.; Triampo, W.; Tang, I-M.; Tieleman, D. P.; Monticelli, L. *Nature Nanotechnol.* **2008**, *3*, 363.
(21) Lee, H.; de Vries, A. H.; Marrink, S.-J.; Pastor, R. W. *J. Phys. Chem. B* **2009**, *113*, 13186.
(22) Kenkare, N. R.; Smith, S. W.; Hall, C. K.; Khan, S. A. *Macromolecules* **1998**, *31*, 5861.
(23) Heine, D. R.; Grest, G. S.; Lorenz, C. D.; Tsige, M.; Stevens, M. J. *Macromolecules* **2004**, *37*, 3857.
(24) Komarov, P. V.; Yu-Tsung, C.; Shih-Ming, C.; Khalatur, P. G.; Reineker, P. *Macromolecules* **2007**, *40*, 8104.
(25) Yang, W.; Wei, D.; Jin, X.; Liao, Q. *Macromol. Theory Simul.* **2007**, *16*, 548.
(26) Hosono, N.; Masubuchi, Y.; Furukawa, H.; Watanabe, T. *J. Chem. Phys.* **2007**, *127*, 164905.
(27) Svaneborg, C.; Everaers, E.; Grest, G. S.; Curro, J. G. *Macromolecules* **2008**, *41*, 4920.
(28) Lacevic, N.; Gee, R. H.; Saab, A.; Maxwell, R. *J. Chem. Phys.* **2008**, *129*, 124903.
(29) Yagyu, H.; Utsumi, T. *Comput. Mater. Sci.* **2009**, *46*, 286.
(30) Lin, P.-H.; Khare, R. *Macromolecules* **2009**, *42*, 4319.
(31) Duering, E. R.; Kremer, K.; Grest, G. S. *Phys. Rev. Lett.* **1991**, *67*, 3531.
(32) Duering, E. R.; Kremer, K.; Grest, G. S. *J. Chem. Phys.* **1994**, *101*, 8169.
(33) Jorgensen, W. L.; Severance, D. L. *J. Am. Chem. Soc.* **1990**, *112*, 4768.
(34) Jorgensen, W. L.; Maxwell, D. S.; Tirado-Rives, J. *J. Am. Chem. Soc.* **1996**, *118*, 11225.
(35) Zhang, W.; Smith, R.; Lowe, C. *J. Coat. Technol. Res.* **2009**, *6*, 315.
(36) Koral, J. N.; Petropulos, J. C. *J. Paint Technol.* **1966**, *38*, 600.
(37) Klimisch, H. J.; Andreae, M.; Tillman, U. *Regul. Toxicol. Pharmacol.* **1997**, *25*, 1.
(38) BSI, BS *11357—2 Plastics - Differential Scanning calorimetry (DSC) - Part 2: Determination of glass transition temperature*; British Standards Institution: Milton Keynes, U.K., 1999.
(39) BSI, BS *527—1 Plastics - Determination of tensile properties - General principles.*; British Standards Institution: Milton Keynes, U.K., 1996.
(40) BSI, BS *527—3 Plastics - Determination of tensile properties - Test conditions for films and sheets.*; British Standards Institution: Milton Keynes, U.K., 1996.

(41) Foster, G. M.; Ritchie, S.; Evans, K. E.; Lowe, C. *Progr. Org. Coat.* **2004**, *51*, 244.
(42) Hagan, E. *Mech. Time Dep. Mater.* **2009**, *13*, 149.
(43) Gabbott, P. *Principles and applications of thermal analysis*; Blackwell Publishing Ltd.: Oxford, U.K., 2008.
(44) Menard, K. P. *Dynamic Mechanical Analysis: A Practical Introduction*; CRC Group: Boca Raton, FL, 2008.
(45) Blomqvist, J.; Pietilä, L.-O.; Mannfors, B. *Polymer* **2001**, *42*, 109.
(46) Ahjopalo, L.; Österholm, H.; Järvinen, H.; Pietilä, L.-O. *Polymer* **2000**, *41*, 8283.
(47) Doi, M.; Edwards, S. F. *The Theory of Polymer Dynamics*; Oxford Science Publications: Oxford, U.K., 1986.
(48) Zhang, W. R.; Zhu, T. T.; Smith, R.; Lowe, C. *Progr. Org. Coat.* **2010**, *69*, 376.
(49) Ward, I. M. *Mechanical Properties of Solid Polymers*; John Wiley and Sons Inc.: New York, 1983.
(50) Plazek, D. J. *J. Rheol.* **1996**, *40*, 987.
(51) Williams, M. L.; Landel, R. F.; Ferry, J. D. *J. Am. Chem. Soc.* **1955**, *77*, 3701.
(52) Ward, I. M.; Sweeney, J. *An Introduction to the Mechanical Properties of Solid Polymers*; John Wiley and Sons Ltd.: New York, 2004.
(53) Lyubartsev, A. P.; Laaksonen, A. *Phys. Rev. E* **1995**, *51*, 3730.
(54) Reith, D.; Müller-Plathe, F. *J. Comput. Chem.* **2003**, *24*, 1624.
(55) Papakonstantopoulos, G. J.; Riggleman, R. A.; Barrat, J.-L.; de Pablo, J. J. *Phys. Rev. E* **2008**, *77*, 041502.
(56) Izvekov, S.; Voth, G. A. *J. Chem. Phys.* **2006**, *125*, 151101.
(57) Milano, G.; Müller-Plathe *J. Phys. Chem. B* **2005**, *39*, 18609.
(58) Harmandaris, V. A.; Kremer, K. *Macromolecules* **2009**, *42*, 791.
(59) Gautieri, A.; Russo, A.; Vesentini, S.; Redaelli, A.; Buehler, M. J. *J. Chem. Theor. Chem.* **2010**, *6*, 1210.
(60) Fitz, B. D.; Mijovic, J. *Macromolecules* **2000**, *33*, 887.
(61) Glatz-Reichenbach, J. K. W.; Sorriero, L.; Fitzgerald, J. J. *Macromolecules* **1994**, *27*, 1334.
(62) Roland, C. M. *Macromolecules* **1994**, *27*, 4242.
(63) Ngai, K. L.; Roland, C. M. *Macromolecules* **1993**, *26*, 6824.
(64) Qazvini, N. T.; Mohammadi, N. *Polymer* **2005**, *46*, 9088.
(65) Hill, L. W. *Paint and Coating Testing Manual - Dynamic mechanical and tensile properties*; ASTM: Philadelphia, PA, 1995.
(66) Zosel, A. *Prog. Org. Coat.* **1980**, *8*, 47.
(67) Radhakrishnan, C. K. *J. Polym. Res.* **2008**, *15*, 161.
(68) The statistical error on the value of E (calculated as the standard deviation of the stress data from their fit values) is of the order of a few MPa for all the samples and temperatures considered. A more conservative error estimate can be obtained by performing three different fitting procedures (F1, F2, F3) for each stress−strain curve. F1 includes all the stress−strain data in the fit, and provides our estimate of the Young's modulus. F2 and F3 include only the peaks of the stress−strain curve lying above (F2) and below (F3) the curve identified by F1. The difference between the slope of the F2 and F3 fit curves is thus used to estimate the indeterminacy with which E is known. In the left panel of Figure 8, the area delimited by F2 and F3 for the stress−strain curve of our cross-linked sample, at temperature of 360 K, is shadowed in light gray. This procedure has been used to derive the error bars plotted in the right panel of Figure 8.